Fatigue Life Prediction of Polycrystals under Multiaxial Straining

Gustavo M. Castelluccio[1,*], David L. McDowell[1,2]

[1] Woodruff School of Mechanical Engineering

[2] School of Materials Science and Engineering

Georgia Institute of Technology, 771 Ferst Drive, N.W, Atlanta, Georgia 30332, USA

* Corresponding author: castellg@gatech.edu

Abstract: In the high cycle fatigue, the initiation of fatigue cracks is significantly affected by microstructure, loading conditions, and specimen geometry. However, fatigue life estimation traditionally considers microstructure and geometric effects via semi-empirical methods without explicit consideration of the early stages of crack formation, which tends to dominate the total lives in high cycle fatigue. Such a strategy has been useful for existing materials that have been characterized with extensive fatigue experiments, but is less applicable to the design of fatigue-resistant alloys or modification of existing alloy microstructures to enhance fatigue resistance. This paper employs a framework developed to assess the early stages of crack formation and growth through the microstructure in smooth and notched specimens. The methodology employs finite element simulations that render an unimodal grain-size microstructure and a crystal plasticity-based fatigue model that estimates 3D transgranular fatigue growth on a grain-by-grain basis. The crystal plasticity model parameters were calibrated for Ni-base superalloy RR1000. In these simulations, cracks form in near surface grains with highest slip-based driving force and then propagate through the field of adjacent grains.

Keywords Fatigue Indicator Parameter, Microstructurally Small Cracks, Fatigue Life

1 Introduction

In spite of its significance in industrial applications, the influence of microstructure on the early stages of fatigue cracks in engineering alloys is still poorly understood. The formation and early growth of fatigue cracks can consume a significant portion of the high cycle fatigue life and is strongly influenced by the size and shape of grains, and the crystallographic orientation. Fatigue models have been able to predict the fatigue life as a function of the microstructure by employing parameters aimed at reflecting the role of microstructure without strong physical connections. These methodologies can assess and perhaps compare materials, but they are not fully appropriate to design of fatigue-resistant engineering alloys.

During the past decade computational simulations have been increasingly used for designing materials. These models simulate microstructure-sensitive mechanical responses with the aim of reducing experimental effort. Castelluccio [1][2] developed a computational methodology for predicting the number of fatigue cycles required to crack an individual grain with highest driving force. The algorithm employs finite element simulations and a crystal plasticity framework to compute nonlocal fatigue indicator parameters (FIPs) which are correlated with the cycles required to crack a grain. This methodology has been successfully employed to assess the effect of bimodal

grain size distributions on fatigue resistance [2].

This work employs similar fatigue and crystal plasticity models to assess the effect of multiaxial straining and stress concentration on early fatigue life. The finite element simulations are calibrated to represent RR1000 Ni-base superalloy and render the microstructure explicitly. The fatigue lives are correlated to a variant of the Fatemi-Socie FIP that is averaged over nonlocal volumes that are oriented as bands aligned with the crystallographic slip planes. The model considers the influence of grain size effects for fatigue cracks that nucleate and extend into neighboring grains.

2 Modeling and simulation

2.1 Constitutive model

At the scale of individual grains we employ a physically-based crystal plasticity constitutive model for RR1000 superalloy adapted from the work of Lin et al. [3]. The crystallographic shearing rate is given by

$$\dot{\gamma}^{(\alpha)} = \dot{\gamma}_0 \exp\left[-\left(\frac{F_0}{k_b T}\right)\left\langle 1-\left\langle \frac{\left|\tau^{(\alpha)}-B^{(\alpha)}\right|-S^{(\alpha)}\mu/\mu_0}{\tau_0\mu/\mu_0}\right\rangle^{p}\right\rangle^{q}\right] sgn\left(\tau^{(\alpha)}-B^{(\alpha)}\right), \quad (1)$$

in which $\dot{\gamma}^{(\alpha)}$ is the shearing rate of slip system α, $\tau^{(\alpha)}$ is the resolved shear stress, T is the absolute temperature, F_o, p, q, $\dot{\gamma}_0$, τ_0, μ, and μ_0 are material parameters that may differ for octahedral and cube slip systems, as listed in Table 1 for 650°C, and k_b is Boltzmann's constant. The evolution laws for slip resistance ($S^{(\alpha)}$) and back stress ($B^{(\alpha)}$) are written as

$$\dot{S}^{(\alpha)} = \left[h_S - d_D\left(S^{(\alpha)} - S_0^{(\alpha)}\right)\right]\left|\dot{\gamma}^{(\alpha)}\right|, \quad (2)$$

$$\dot{B}^{(\alpha)} = h_B\dot{\gamma}^{(\alpha)} - r_D^{(\alpha)}B^{(\alpha)}\left|\dot{\gamma}^{(\alpha)}\right|, \quad (3)$$

in which $r_D^{(\alpha)} = \frac{h_B\mu_0}{S^{(\alpha)}}\left\{\frac{\mu_0'}{f_c\lambda}-\mu\right\}^{-1}$ and S_0, h_B, h_S, d_D, μ_0', f_c, λ, are constants that differ for octahedral and cube slip planes (see Table 1). The initial values are specified as S_0 for the slip resistance and zero for the back stress. This formulation considers 12 octahedral and 6 cube slip systems and was implemented as a user-material subroutine (UMAT) in ABAQUS 6.9 [4] using an implicit integration scheme. Discussion of model parameters and their estimation can be found in Ref. [1].

2.2 Fatigue driving force

During crack nucleation and early growth, the local fatigue driving force is affected by the microstructure, which has particular implications for microstructurally small cracks (MSCs). Hence,

Table 1. Parameters of the constitutive model at 650°C for octahedral and cube slip systems.

	F_0 kJ/mol	p	Q	$\dot{\gamma}_0\, s^{-1}$	τ_0 *GPa*	S_0 *MPa*	f_c	h_B *GPa*	h_S *GPa*	d_D *MPa*	$\mu_0' GPa$
Oct.	295	0.31	1.8	120	810	350	0.42	400	10	6024	72.3
Cube	295	0.99	1.6	4	630	48	0.18	100	4.5	24	28.6

Other: λ=0.85, μ_0' = 192GPa. Elastic constants: C_{11} = 166.2GPa, C_{12} = 66.3GPa, C_{44} = 138.2GPa.

the driving force for early stage fatigue needs to be characterized with fatigue indicator parameters (FIPs) describing the local fields (rather than far field basis of the stress intensity factor in LEFM). The present approach quantifies the driving force with a crystallographic version of the Fatemi-Socie parameter adapted to evaluate the FIP on each octahedral slip system, i.e.,

$$\mathrm{FIP}^{\alpha} = \frac{\Delta\gamma_p^{\alpha}}{2}\left(1 + k\frac{\sigma_n^{\alpha}}{\sigma_y}\right) \tag{4}$$

where $\Delta\gamma_p^{\alpha}$ is the cyclic plastic shear strain range on slip system α, σ_n^{α} is the peak stress normal to this slip system, σ_y is the cyclic uniaxial yield strength of the polycrystal, and *k=0.5*, as proposed by Fatemi and Socie [5]. Several investigators have successfully employed approaches akin to the Fatemi-Socie parameter along with crystal plasticity formulations for studying the effects of microstructure on fatigue life [6][7]. The value of such a parameter was further explored by Reddy and Fatemi [8], who postulated that the Fatemi-Socie parameter represents the fatigue driving force and plays a role similar to that of the ΔK or the ΔJ in predicting fatigue crack formation and early growth. Recently, Castelluccio and McDowell [9] correlated the Fatemi-Socie parameter with the cyclic crack tip displacement using crystal plasticity simulations. To numerically regularize the FEM discretization and also to represent the finite physical scale of the fatigue damage process zone, the FIP^{α} values are calculated at each integration point and then averaged along bands (i.e., nonlocal FIPs), parallel to slip planes across entire grains, as depicted in Figure 1.

2.2.1 Life estimation

This approach focuses on the interaction between small fatigue cracks and the microstructure at a mesoscale level; therefore, crack growth on a grain-by-grain basis. In other words, the number of cycles to crack the first grain (nucleation) is first computed, and then the cycles required to extend the microstructurally small crack within each of the neighboring grains is computed. Each nonlocal FIP is employed in fatigue life correlations using a hierarchical approach to estimate the life to completely crack a grain along a band. The nucleation relation is assumed to follow the semi-empirical empirical law [6]

$$N_{nuc} = \frac{\alpha_g}{d_{gr}}(FIP^{\alpha})^{-2}\,, \tag{5}$$

where α_g is an irreversibility coefficient and d_{gr} is a length scale of the current grain calculated as:

$$d_{gr} = D_{st} + \sum_{i}^{n} \omega^i D_{nd}{}^i, \tag{6}$$

in which ω^i is the disorientation factor for grain i, D_{st} is related to the length of the band considered and D^i_{nd} relates to the length of all n intersecting bands in adjacent grains. The values of D_{st} and D^i_{nd} are calculated for each averaging band as the square root of the area of the band. The disorientation factor is computed as

$$\omega = \left\langle 1 - \frac{\theta_{dis}}{20^o} \right\rangle \tag{7}$$

Here, θ_{dis} is the disorientation angle between two grains, and the Macaulay brackets satisfy that $<a>=a$ if $a > 0$, $<a>=0$ if $a \le 0$. Thus, ω = 1 when there is no disorientation (i.e., the grain and the neighbor have exactly the same orientation and should be a single grain) and ω = 0 if the disorientation is 20° or larger. The disorientation factor for randomly oriented grains results in non-zero values for fewer than 10% of the grain boundaries.

The MSC crack growth rate is assumed to be controlled by the mechanical irreversibility of dislocations emitted from the crack tip and proportional to the crack tip displacement range, i.e.,

$$\left.\frac{da}{dN}\right|_{msc}^{\alpha} = \phi \left\langle A \quad \mathrm{FIP}^{\alpha} - \Delta \mathrm{CTD}_{\mathrm{th}} \right\rangle, \tag{8}$$

where $(A \sim 2)$ is a scaling constant that depends on microstructure attributes, $\Delta \mathrm{CTD}_{\mathrm{th}}$ is a threshold that has a value close to the magnitude of the Burgers vector. The factor $\phi=0.077$ measures the mechanical irreversibility at the crack tip process zone and depends on environment. The number of cycles to extend the crack front through the i^{th} grain along slip system α in the MSC regime, $N_{G_i}|_{MSC}^{\alpha}$, is determined by integrating Equation (8) with respect to the crack length. The crack growth rate

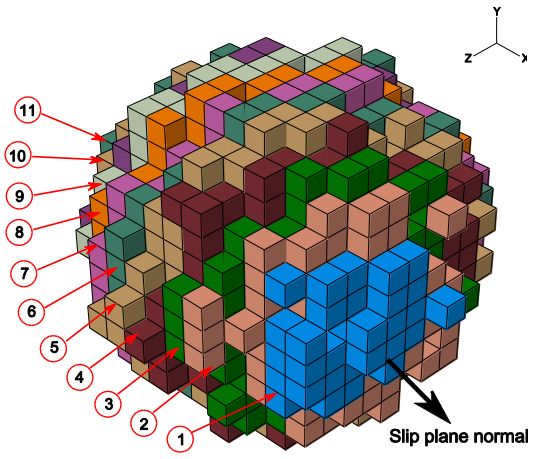

Figure 1: Schematic representation of elements, bands and grains in which FIPs are averaged to estimate transgranular fatigue crack growth. The implementation in a FEM model with unstructured, voxellated meshing is shown, with bands color coded and numbered for a single spherical grain.

depends on the crack length/size within the i^{th} grain, which varies from an uncracked to a fully cracked grain. To integrate analytically Equation (8), we consider that the mean evolution of FIP^{α} inside the grain follows a decreasing law, i.e.,

$$\mathrm{FIP}^{\alpha} = \mathrm{FIP}_o^{\alpha}\left(1-\frac{1}{2}a_i^2\right) \tag{9}$$

Here, a_i is defined here as the *fraction* of the area of the i^{th} grain to have cracked (nondimensional measure of cracked area of slip plane within the grain), and FIP_o^{α} represents the FIP value for the i^{th} grain on the α^{th} slip system along which a_i is measured, *before the grain is cracked*. Interestingly, Equation (9) resembles the empirical laws proposed by Hobson et al. [10] [11] and Miller [12] and has been validated using FEM simulations [1].

After integrating, the total life consumed in the MSC regime (N_{MSC}) is the sum of the lives for each grain involved in the growth process for a given 3D crack, i.e.,

$$N_{MSC} = \sum_i N_i\,|_{MSC}^{\alpha} \,. \tag{10}$$

where
$$N_i\,|_{MSC}^{\alpha} = N_{G_i}\,|_{MSC}^{\alpha} - N_{History} = \frac{1}{\sqrt{c_1 c_2}}\tanh^{-1}\left(D_{st}\sqrt{\frac{c_2}{c_1}}\right) - N_{History} \tag{11}$$

$$c_1 = \phi\,\frac{D_{st}+\sum_i^n \omega^i D_{nd}{}^i}{d_{gr}^{ref}}\,2\mathrm{FIP}_0^{\alpha} - \phi\,\Delta\mathrm{CTD}_{th} \quad \text{and} \quad c_2 = \phi\,\frac{\mathrm{FIP}_0^{\alpha}}{\left(D_{st}+\sum_i^n \omega^i D_{nd}{}^i\right) d_{gr}^{ref}} \tag{12}$$

Here, $N_{History}$ corresponds to the number of cycles undergone since the band considered has intersected the crack perimeter, and is necessary to include since cracks grow in multiple grains along a 3D crack front. Further details can be found in Refs. [1][2].

2.3 Crack growth model

To compute stress redistribution due to an increment in crack length, we employ an isotropic damage model along the bands having FIP values that lead to minimum fatigue lives. For the elements within these bands, the elastic stiffness tensor $\bar{\mathbf{C}}$ is degraded according to damage parameter d_1, i.e.,

$$\bar{\mathbf{C}} = (1-d_1)\mathbf{C} \tag{13}$$

Here, d_1 varies from 0 (uncracked) to 0.99, at which point full damage is assumed. The elastic stiffness is degraded for those elements in bands along which the crack is assumed to grow. The degradation of the elastic stiffness requires a gradual increase of parameter d_1 to achieve convergence of the FEM solution. Accordingly, the degradation is imposed over several time steps, i.e., for the current time step Δt^i we write

$$d_1^{(i+1)} = d_1^{(i)} \pm \nu \, \Delta t^i \tag{14}$$

For example, a value of $\nu = 2$ was enough to increase d_1 up to 0.99 by the end of the 1-second half loading cycle; of course, ν can be varied to accelerate crack stiffness reduction and to allow for convergence while computing stress redistribution effects in the polycrystal over a few computational cycles. Of course, this represents evolution over a much larger number of applied fatigue loading cycles. The plus sign corresponds to the case in which the stress normal to the band is positive and the crack plane is in tension. On the contrary, if the stress normal to the band is in compression, the crack is assumed to be closed and d_1 is decreased to zero at a rate proportional to the time step, as described by the minus sign in Equation (14).

When roughness- or plasticity-induced closure conditions are detected by virtue of compressive traction normal to the crack face on individual elements, the value of d_1 is decreased to 0 such that the initial elastic stiffness is restored. Hence, the degradation of the stiffness tensor is performed on a grain-by-grain basis by increasing the parameter d_1 in all the elements after predicting the path of the crack in the following grain. Such a prediction is performed every two computational loading cycles to allow for stiffness degradation and the update of the stress and strain fields.

In summary, the fatigue algorithm starts by calculating the nonlocal FIP values on every band in every grain over the third computational cycle, and proceeds by calculating the number of expected cycles to nucleate crack on all bands for all grains using Equation (5). The elements within the band with the lowest nucleate life are marked as "cracked," and the model applies again a couple of computational loading cycles to update the FIP values and to degraded (d_1 increased) the stiffness tensor as necessary to represent crack growth. Thereafter, the algorithm computes the MSC life of all FIP averaging bands that intersect the crack perimeter and renders the elements in the band with minimum life as cracked. The simulation proceeds by applying further loading cycles, in which the stiffness tensor is degraded on the cracked elements to redistribute stress and plastic strain, while checking for grain level closure effects of cracked grains, and the MSC life is evaluated again on the remaining grains. Since we seek to describe the dominant crack, only one crack nucleates per realization.

3 Simulation results

3.1 Specimens and loading conditions

Figure 2 depicts the C3D8R-element meshes employed for modeling smooth and notched specimens, each color representing a different crystallographic orientation. The grain size follows a lognormal distribution based on the algorithm by Musinski [13] with a mean value of 18μm. The straining sequence consisted of triangular relative displacement of the upper and lower boundary planes at a 0.05%/s strain rate under shear or tensile mode loading to achieve an overall nominal strain range of 0.8%; lateral faces are free of traction. Simulations with different strain ratios employed a similar strain range to assess only the effect of applied strain ratios (strain/displacement conditions).

To achieve equivalence with tensile straining, the magnitude of the displacement vector in shear straining was computed by assuming an elastic model with cubic symmetry. The value of Poisson's

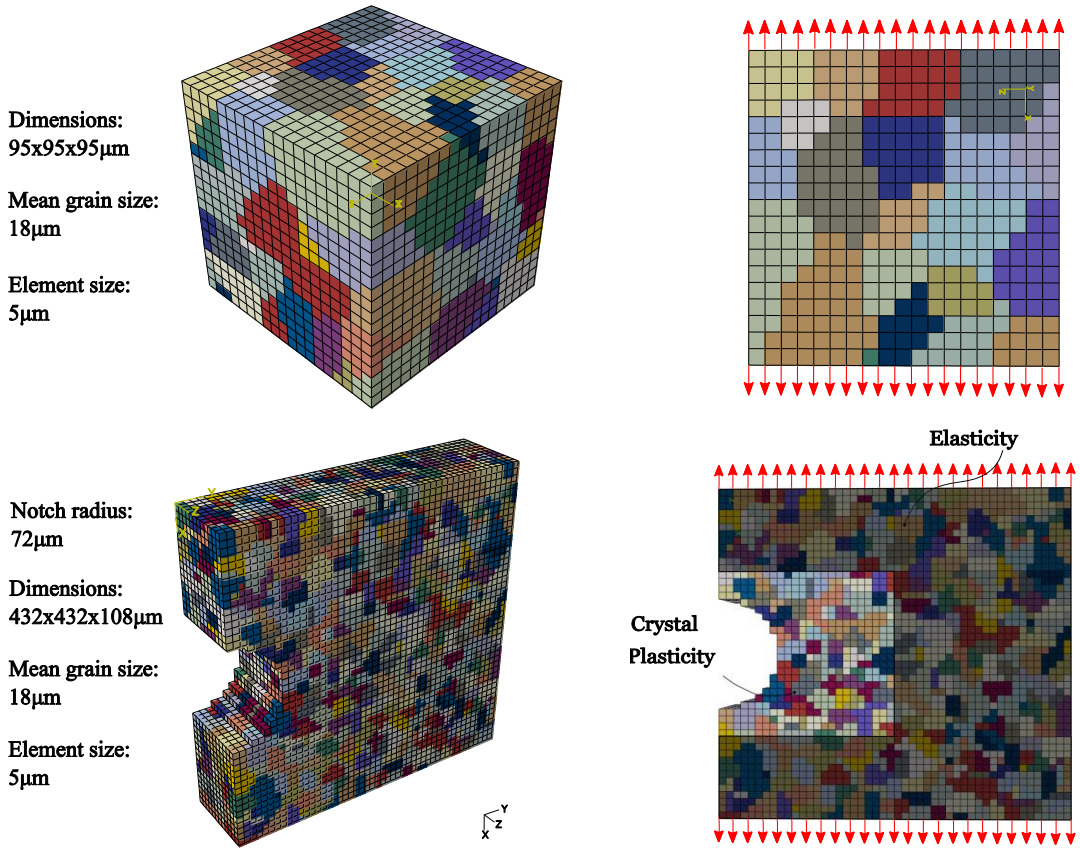

Figure 2. Example of voxellated meshes representing the explicit polycrystalline microstructure for axial straining of smooth (top) and notched (bottom) specimens. Triangular straining sequence is applied by displacing the upper and bottom faces of the meshes at 0.05%/s strain rate.

ratio was deduced to compute the equivalent pure shear strain for $R_\varepsilon = 0$. The 0.8% uniaxial strain range is equivalent in shear to

$$\Delta\gamma_{eq} = (1+\nu)\Delta\varepsilon_1 = (1+\nu)0.8\% = (1+0.3989)0.8\% = 1.119\% \tag{15}$$

Thus, the upper and lower faces were displaced in shear up to a nominal shear strain of 1.119% for equivalence in this particular case. The Poisson's ratio was deduced using an elastic model with cubic symmetry, i.e.,

$$\nu = \frac{C_{12}}{C_{11}} = \frac{66.3}{166.2} = 0.399 \tag{16}$$

3.2 Crack growth vs cycles for smooth specimens

Smooth specimens were employed to simulate shear and tension-compression straining at 650°C for under three strain ratios $R_\varepsilon = \varepsilon_{min} / \varepsilon_{max}$ = -1, R_ε = 0 and R_ε = 0.5, all undergoing an equivalent nominal strain range of 0.8% at 0.05%/s strain rate. For each loading condition, a total of 10 equivalent microstructure realizations were simulated. The simulations considered unidirectional periodic boundary conditions, with lateral faces free of traction. Figure 3 presents crack length vs. life on a semi-log scale. Each data point corresponds to extending the crack by one grain and only lives below 10^9 are considered (otherwise considered as crack arrest, giving rise to run-out

behavior). These results support that uniaxial tension-compression straining is more detrimental than cyclic shear, by a factor of nominally two or greater on life.

Fatigue crack nucleation rather than fatigue crack growth seems particularly influenced for $R_\varepsilon = 0$ and $R_\varepsilon = 0.5$, which suggests that crack nucleation assisted by stress concentration (e.g., notch, pore, or inclusion) might exhibit a reduced dependence on the strain ratio. Furthermore, tension-compression fatigue life results seem to show slightly less variability, and for both displacement conditions, the variability seems to increase with decreasing strain ratio.

Figure 4 presents an example of the stress-strain evolution for one realization in tension after 20 straining cycles for three different strain ratios. As expected, higher strain ratios lead to higher tensile mean stresses. The mean stress evolves slowly and after 20 cycles the change is less 10%; therefore we may consider that the fatigue life estimations are performed at a relatively stable mean stress level for each strain ratio. Even when mean stress assessed may differ from a fully relaxed state, the fatigue model was calibrated under similar conditions [1], which reduces the inaccuracies.

3.3 Crack growth vs cycles for notched specimens

Figure 5 presents the simulation results for three strain ratios using models with a notch root radius of 144 μm and a similar microstructure. Compared to the smooth specimens, the results from models with a notch show a reduction in fatigue life of about an order of magnitude. As expected, the lower the strain ratio, the larger the fatigue life, while tension-compression simulations resulted in lower lives than shear loading. However, the separation in life between tension-compression and shear cases increases with decreasing strain ratio, which was not clearly observed in simulations with smooth specimens. Note that the cracks for the shear case did not nucleate at the notch, but grew in the bulk of the specimen. The computed results for tension-compression, which nucleated the crack at the notch, lie within two orders of magnitude on life. In the case of shear loading, the life is longer and exhibits greater scatter as the cracks formed in the bulk of the specimen.

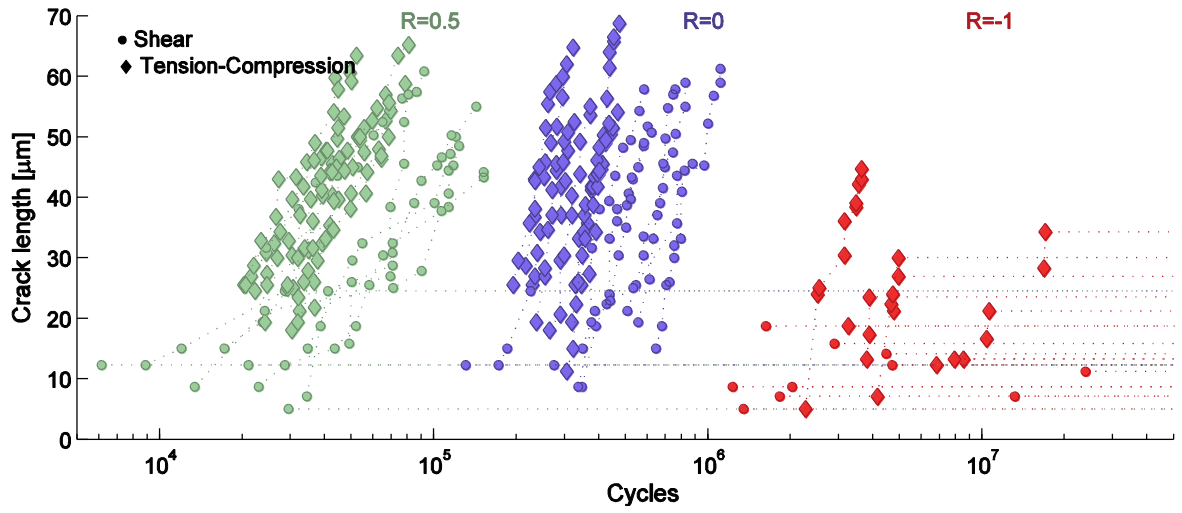

Figure 3. Comparison of the results for strain ratios $R_\varepsilon = 0$, $R_\varepsilon = 0.5$ and $R_\varepsilon = -1$ using simulations with unidirectional periodic conditions undergoing an equivalent nominal strain range of 0.8%.

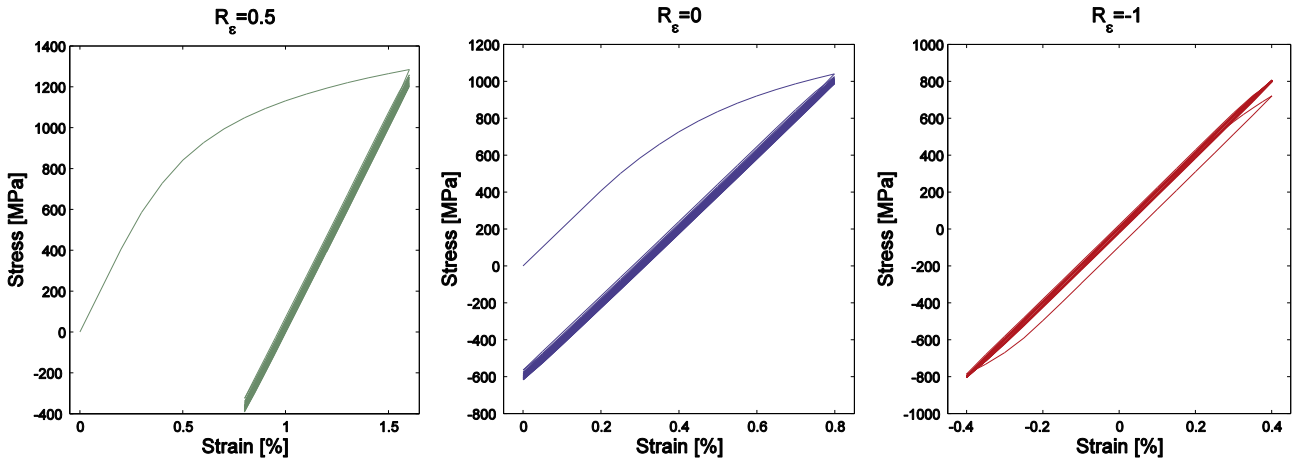

Figure 4. Stress-strain responses of a smooth specimen microstructure realization and three strain ratios over 20 uniaxial straining cycles.

4 Discussion and conclusions

The simulations showed quantitatively the detrimental effects of higher strain ratios, which change orders of magnitude the cycles required to grow a crack of similar lengths. Furthermore, in all cases tension-compression straining was more damaging than shear straining, which has been reported in the literature for other materials [14][15]. The results for smooth specimens exhibited a spread of fatigue life over three orders of magnitude for strain ratios between $R_\varepsilon = 0.5$ and $R_\varepsilon = -1$, for shear and tension-compression loading. Notched specimens under tension-compression loading showed a smaller spread, which is explained by a reduction of the variability in nucleating a crack. This effect dominates over the reduction of the highly strained volume around the notch. In the case of notches under shear, the cracks nucleated within the bulk of the specimen (not at the notch), and the results are comparable to those found for smooth specimens.

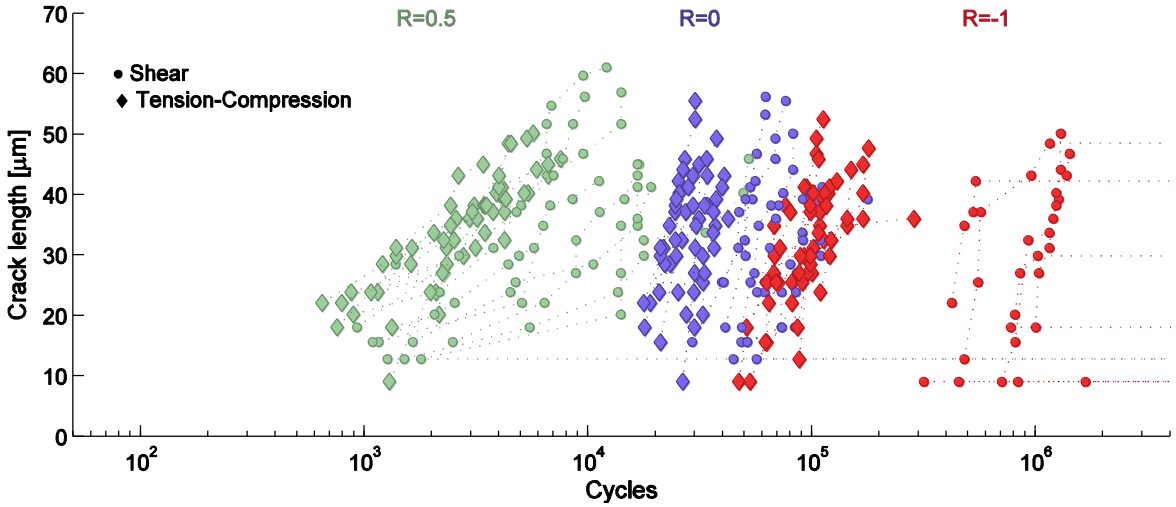

Figure 5. Comparison of the results for strain ratios $R_\varepsilon = 0$, $R_\varepsilon = 0.5$ and $R_\varepsilon = -1$ on a logarithmic scale for notched specimens undergoing an equivalent nominal strain range of 0.8%.

Acknowledgements

G. M. Castelluccio and D.L. McDowell are deeply grateful for the support provided by Integrated Systems Solutions, Inc. (Technical Monitor: Dr. Nam Phan, NAVAIR).

References

[1] G. M. Castelluccio, 'A study on the influence of microstructure on small fatigue cracks', PhD Thesis, Georgia Institute of Technology, Atlanta, GA, USA, 2012.

[2] G. Castelluccio, D. L. McDowell, 'Fatigue Life Prediction of Microstructures'. In *Proceedings of the ASME International Mechanical Engineering Congress and Exposition*. Houston, Texas, USA: ASME, 2012.

[3] B. Lin, L. G. Zhao, J. Tong, and H.-J. Christ, 'Crystal plasticity modeling of cyclic deformation for a polycrystalline nickel-based superalloy at high temperature', *Mater. Sci. Eng., A,* 527(15), 3581–3587, 2010.

[4] ABAQUS, *FEM software V6.9, Simulia Corp., Providence, RI, USA*. Providence, RI, USA: Simulia, Inc., 2009.

[5] A. Fatemi, D. F. Socie. A critical plane approach to multiaxial fatigue damage including out-of-phase loading. *Fatigue Fract. Eng. Mater. Struct.*, 11(3), 149--165, 1988.

[6] M. Shenoy, J. Zhang, and D. L. McDowell, "Estimating fatigue sensitivity to polycrystalline Ni-base superalloy microstructures using a computational approach," *Fatigue Fract. Eng. Mater. Struct.*, (10) , 889-904, 2007.

[7] C. Przybyla, R. Prasannavenkatesan, N. Salajegheh, and D. L. McDowell, 'Microstructure-sensitive modeling of high cycle fatigue', *Int. J. Fatigue*, 32 (3), 512–525, 2010.

[8] S. C. Reddy and A. Fatemi, 'Small Crack Growth in Multiaxial Fatigue', in *Advances in Fatigue Lifetime Predictive Techniques*, ASTM, 1992, 276–298.

[9] G. M. Castelluccio and D. L. McDowell, "Assessment of Small Fatigue Crack Growth Driving Forces in Single Crystals with and without Slip Bands, *Int. J. Fracture*, 176(1), 49-64 2012.

[10] P. D. Hobson, "The formulation of a crack-growth Equation for short cracks," *Fat. Eng. Mater. Struct.*, 5 (4) , 323-327, 1982.

[11] P. D. Hobson, M. W. Brown, and E. R. de los Rios, "Two Phases of Short Crack Growth in a Medium Carbon Steel," in *The behaviour of short fatigue cracks* (London: Mechanical Engineering Publications, 1986), 441-459.

[12] K. Miller, "The three thresholds for fatigue crack propagation," in *Fatigue and Fracture Mechanics: 27th volume*, ASTM STP 1296 (1997), 267-286.

[13] W. D. Musinski, D. L. McDowell, Microstructure-sensitive probabilistic modeling of HCF crack initiation and early crack growth in Ni-base superalloy IN100 notched components. *Int. J. Fatigue*, 37, 41–53, 2012.

[14] F. A. Kandil, M. W. Brown, and K. J. Miller. "Biaxial Low Cycle Fatigue Failure of 316 Stainless Steel at Elevated Temperatures," In *Metal Society Book 280*, 203–210. Varese, Italy: Metal Society of London, 1982.

[15] H. A. Suhartono , K. Pötter, A. Schram, and H. Zenner. "Modeling of Short Crack Growth Under Biaxial Fatigue: Comparison Between Simulation and Experiment," 323–339. ASTM STP 1387, 2000.